CHAPTER ONE

DNA Translocation of ATP-Dependent Chromatin Remodeling Factors Revealed by High-Resolution Optical Tweezers

Yongli Zhang[1], George Sirinakis, Greg Gundersen, Zhiqun Xi, Ying Gao

Department of Cell Biology, Yale University School of Medicine, New Haven, Connecticut, USA
[1]Corresponding author: e-mail address: yongli.zhang@yale.edu

Contents

Abstract

ATP-dependent chromatin remodeling complexes (remodelers) use the energy of ATP hydrolysis to regulate chromatin structures by repositioning and reconfiguring

Methods in Enzymology, Volume 513
ISSN 0076-6879
http://dx.doi.org/10.1016/B978-0-12-391938-0.00001-X

nucleosomes. Ensemble experiments have suggested that remodeler ATPases are DNA translocases, molecular motors capable of processively moving along DNA. This concept of DNA translocation has become a foundation for understanding the molecular mechanisms of ATP-dependent chromatin remodeling and its biological functions. However, quantitative characterizations of DNA translocation by representative remodelers are rare. Furthermore, it is unclear how a unified theory of chromatin remodeling is built upon this foundation. To address these problems, high-resolution optical tweezers have been applied to investigate remodeler translocation on bare DNA and nucleosomal DNA substrates at a single-molecule level. Our strategy is to hold two ends of a single DNA molecule and measure remodeler translocation by detecting the end-to-end extension and tension changes of the DNA molecule in response to chromatin remodeling. These single-molecule assays can reveal detailed kinetics of remodeler translocation, including velocity, processivity, stall force, pauses, direction changes, and even step size. Here we describe instruments, reagents, sample preparations, and detailed protocols for the single-molecule experiments. We show that optical tweezer force microscopy is a powerful and friendly tool for studies of chromatin structures and remodeling.

1. INTRODUCTION

Remodelers are a large family of protein complexes involved in all DNA-related transactions in eukaryotes, including gene transcription, replication, recombination, and repair (Bowman, 2010; Clapier & Cairns, 2009; Hargreaves & Crabtree, 2011; Smith & Peterson, 2005). They contain evolutionarily conserved and specialized ATPase motors and perform common and diverse catalytic activities and biological functions (Flaus, Martin, Barton, & Owen-Hughes, 2006). Based on the sequence homology of their ATPases, remodelers belong to the SWI2/SNF2 family of the SF2 helicase/translocase superfamily and can be further divided into the SWI/SNF-like, ISWI, Mi-2/CHD, and INO80 subfamilies (Clapier & Cairns, 2009). Besides the catalytic ATPase domains, remodelers contain various accessory protein domains or subunits that help remodelers bind onto nucleosomes, interact with transcription factors, recognize histone modifications or variants, and regulate remodeler activities. This modular structure allows remodelers to have both common and diverse functions. All remodelers are capable of mobilizing nucleosomes *in vitro* (Hamiche, Sandaltzopoulos, Gdula, & Wu, 1999; Langst, Bonte, Corona, & Becker, 1999). *In vivo*, remodelers often have overlapping activities (Boeger, Griesenbeck, Strattan, & Kornberg, 2004; Gkikopoulos et al., 2011). However, remodelers can

have important and distinct biochemical functions. Remodelers in the SWI/SNF-like subfamily can disassemble nucleosomes and disrupt folded chromatin structures (Sinha, Watanabe, Johnson, Moazed, & Peterson, 2009), leading to gene activation and recombination. In contrast, remodelers in the ISWI and CHD1 subfamilies can assemble nucleosomes and generally help chromatin folding, resulting in gene repression (Gkikopoulos et al., 2011). Specifically, CHD1 can assemble the histone variant H3.3 into chromatin in a genome-wide, replication-independent manner (Konev et al., 2007). Finally, INO80 and SWR1 can exchange histone H2A in nucleosomes with its variant H2A.Z (Mizuguchi et al., 2004; Papamichos-Chronakis & Peterson, 2008). Thus, remodelers are conserved and specialized molecular machines with important and diverse biological functions (Cairns, 2005).

The molecular mechanisms of ATP-dependent chromatin remodeling are poorly understood. Growing evidence indicates that remodeler ATPases are DNA translocases (Saha, Wittmeyer, & Cairns, 2002). The evidence includes their homology with other translocases or helicases and DNA length-dependent ATPase activities. However, this evidence is rather indirect and obtained only for a few remodelers (Whitehouse, Stockdale, Flaus, Szczelkun, & Owen-Hughes, 2003). Especially, some motors in the SF2 superfamily do not seem to be DNA translocases (Pyle, 2008). Therefore, more direct tests of remodeler translocation are required. We have provided some of the first direct evidence for remodeler translocation using optical tweezers (Zhang et al., 2006). We measured the translocation processivities, velocities, step sizes, and forces of SWI/SNF and RSC on nucleosomal DNA, and the corresponding parameters of a minimal RSC complex on bare DNA (Sirinakis et al., 2011). Interestingly, these remodelers show distinct translocation properties, especially compared to Rad54, a motor protein in the SWI2/SNF2 family involved in DNA recombination and repair (Amitani, Baskin, & Kowalczykowski, 2006). For example, the minimal RSC complex and Rad54 move on DNA with dramatically different average velocities (25 vs. 301 bp/s) and processivities (35 vs. ~11,500 bp). Therefore, despite their conserved structures, SWI2/SNF2 motors have different translocation properties, a fact that is important to understanding their functional diversities.

Optical tweezers generally use one or two optical traps to hold polystyrene or silica beads as force and displacement sensors (Moffitt, Chemla, Smith, & Bustamante, 2008). Optical traps are diffraction-limited light spots formed by focusing collimated laser beams using objectives with high numerical apertures (NAs). The large electric field gradient in the light spot

will polarize small dielectric particles such as polystyrene beads and attract them to the location of highest field intensity, the center of the optical trap. For a small displacement of the bead from the trap center (typically <300 nm for a 2-μm-diameter bead), the restoring force exerted on the bead is proportional to the displacement (Greenleaf, Woodside, Abbondanzieri, & Block, 2005). Thus, the optical trap serves as a harmonic potential for the bead. The force constant of the trap is proportional to the total intensity of the trapping light and can be experimentally measured. Furthermore, optical tweezers contain optoelectronic modules to measure the bead displacement with high resolution based upon an interference method. When attaching the macromolecule of interest to two trapped beads, the beads can serve as excellent force and displacement sensors to report the structure and dynamics of the macromolecule. Therefore, optical tweezers extend our hands and allow us to manipulate single molecules and detect their movements and responses to external forces in real time. As a result, optical tweezers have been widely applied to study molecular motors and structures and dynamics of macromolecules (Bustamante, Cheng, & Mejia, 2011).

In this chapter, we detail single-molecule experiments of remodeler translocation using high-resolution optical tweezers. After an introduction to the optical tweezers, we focus on the translocation of remodelers on bare DNA and nucleosomal DNA.

2. INSTRUMENT

2.1. Instrumentation of high-resolution dual-trap optical tweezers

The instrument was assembled on an optical table using off-the-shelf and custom-made parts, mainly as previously described (Fig. 1.1A) (Moffitt, Chemla, Izhaky, & Bustamante, 2006). Briefly, a single laser beam of 1064 nm is expanded, collimated (by the telescope T1), and split into two orthogonally polarized beams (by PBS2) that are reflected by a rotary mirror (NM) and a stationary mirror, respectively. The two beams are then combined by a polarizing beam splitter (PBS3), further expanded (by the telescope T2), and finally focused deep into water to form two optical traps in a flow cell by a water-immersion microscope objective (FO, Nikon $60\times$ NA $=1.2$). The separation between the two traps can be precisely controlled to adjust the force applied to the molecule of interest, by turning the piezoelectrically controlled rotary mirror (Mad City Labs). To detect bead

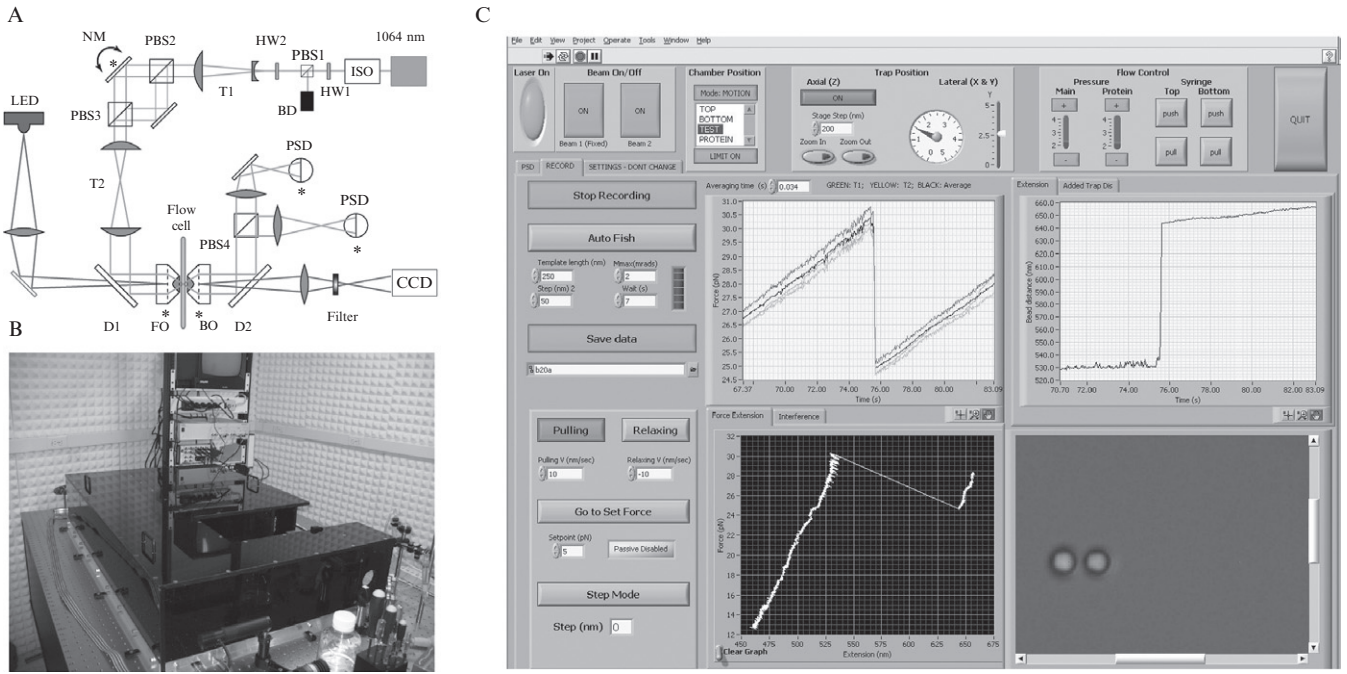

Figure 1.1 High-resolution optical tweezers. (A) Optical diagram of the dual-trap optical tweezers. ISO, optical isolator; HW, half-wave plate; BD, beam dumper; T, telescope; PBS, polarizing beam splitter; NM, piezo mirror; D, dichroic mirror; FO, front objective; BO, back objective. The positions marked by stars represent optically conjugated planes. (B) The enclosed optical paths and components of the tweezers on an optical table in an environmentally controlled room. (C) Labview interface used to remotely operate the optical tweezers.

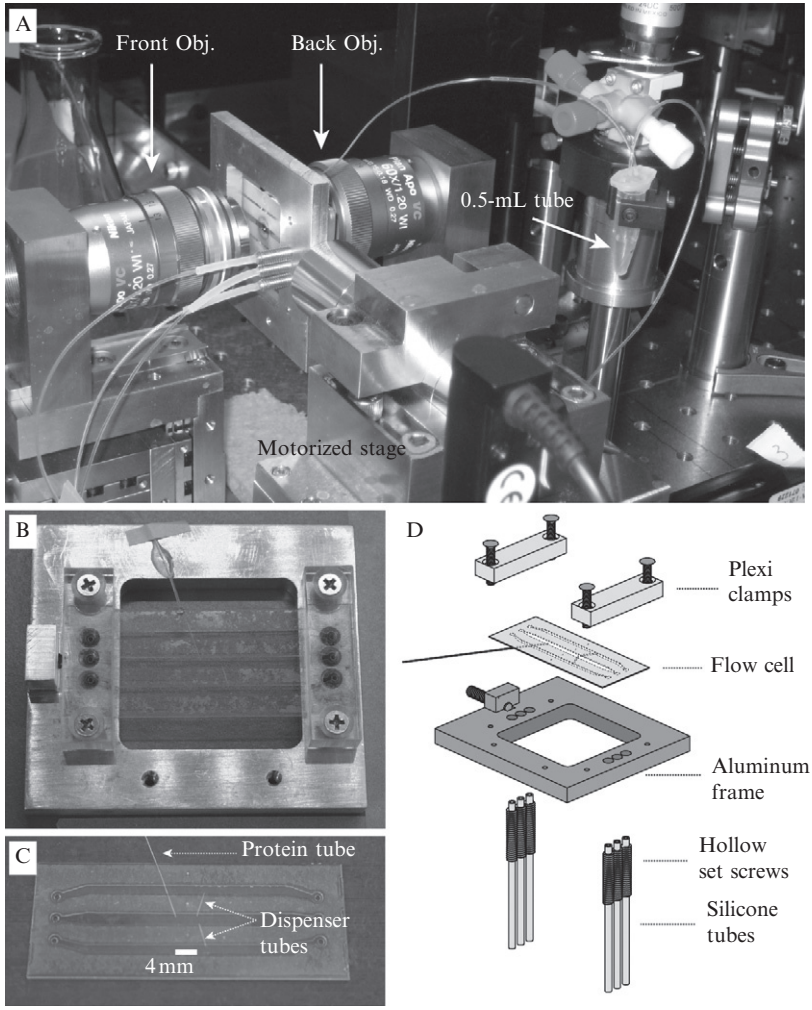

Figure 1.2 Microfluidic system used in the tweezer instrument. (A) Flow cell installed on a motorized stage and positioned between two water-immersion objectives. Tubing connected to the flow cell, including the 0.5-mL microcentrifuge tube containing the remodeler solution, can be seen. (B) Flow cell mounted on a $2.5'' \times 2.75''$ aluminum frame and held in place by two plexi clamps. (C) Picture of an assembled flow cell. It is constructed by sandwiching two nescofilm (Alfresa Pharma Co.) gaskets and three glass tubes between two microscope cover slides ($60 \times 24 \times 0.17$ mm). The nescofilm gasket is cut to create three channels by a laser engraver (Epilog Zing 16 laser system with 30W CO_2 laser, Epilog Laser, CO). The bottom coverslip containing six holes for fluid delivery is cut by the same engraver. The flow cell is then placed onto a hot plate and heated to 75 °C. At this temperature, the nescofilm will not melt, but air bubbles can be removed with small amounts of pressure. The temperature is then increased to 110 °C,

displacement, the outgoing laser light is collimated again by a second identical objective (BO, Fig. 1.2A) and projected to two position-sensitive detectors (PSD, Fig. 1.1A). The detectors have voltage outputs that are proportional to the small lateral bead displacements and can be converted to displacement and force measurements after certain calibrations (Gittes & Schmidt, 1998).

The design of dual-trap optical tweezers has been proven to be robust and immune to many noises. Because the biomolecule of interest is attached between two optically levitated beads and isolated from the microscope stage, experimental measurements, such as the end-to-end extension and tension of the biomolecule, are not affected by stage drift that is sensitive to environmental changes (Nugent-Glandorf & Perkins, 2004). Furthermore, the extension and tension can be measured by the difference between outputs of two PSDs. This differential detection scheme greatly reduces noises common to both traps, such as laser pointing errors, in-phase bead fluctuations, and even residue flows in the fluidic channel. Moreover, the environment for the optical tweezers is carefully controlled (Fig. 1.1B). The optical components of the tweezers are located in an acoustically isolated room with stringent controls in temperature and air flow (Abbondanzieri, Greenleaf, Shaevitz, Landick, & Block, 2005; Moffitt et al., 2006). Noisy equipment is put outside of the tweezer room, including the computer that controls the tweezers and the pumping light source for the diode-pumped solid state laser for optical trapping. As a result, optical tweezers are remotely operated through a Labview interface (Fig. 1.1C) after the sample is loaded. Finally, we found that the quality of the trapping laser is crucial for optical tweezers. Commercially available lasers at 1064 nm should be tested in the lab for good Gaussian beam profiles and stability, using a beam profiler and a power meter, respectively. The beam quality can also be checked by shining part of the beam to a PSD and assessed by taking the power spectrum density of the PSD signal, as is demonstrated in

covered with a hot block, and left for 30 min. The assembled flow cell should be clear, particularly on the edges of the channels and near the holes. The glass tubes are custom made by King Precision Glass, CA, and have diameters of 80 μm (OD) and 40 μm (ID) for the protein injection tube and of 100 μm (OD) and 25 μm (ID) for the dispenser tube. The channels in the flow cell have a thickness of around 180 μm. (D) Diagram showing the assembly of the microfluidic system. Silicone tubes are used to snuggly fit to the holes into the three microfluidic channels when screwed into the aluminum frame.

Fig. 1.3. Using the design described above and taking precautions for the environment and quality of the trapping laser, we and others have built high-resolution optical tweezers reaching base-pair resolution with high baseline stability (Moffitt et al., 2006; Sirinakis et al., 2011). High-resolution and stable optical tweezers are essential for single-molecule studies of remodeler translocation. Because of remodeler's relatively small processivities ($\lesssim 100$ bp) and velocities (< 30 bp/s) (Sirinakis et al., 2011; Zhang et al., 2006), the resultant small changes in DNA extension and tension due to remodeler translocation can only be well distinguished from background noises or baseline drifts by high-resolution optical tweezers.

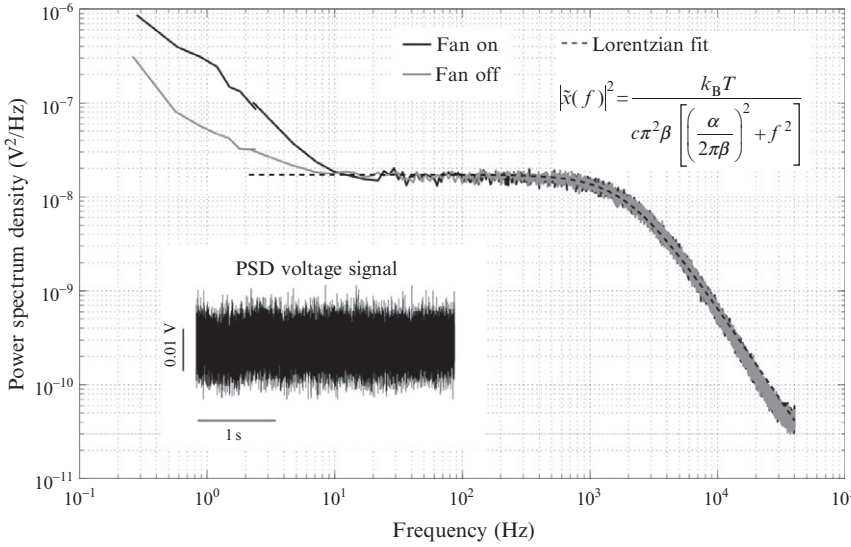

Figure 1.3 Power spectrum density distributions of Brownian motion of the same trapped bead measured when the fan is on (black curve) and off (gray curve). Part of the corresponding PSD output is shown as an inset. The distributions can be well fit with a Lorentzian function (dashed line shown for fan off) in the range of 10–10^4 Hz. The Lorentzian function is expressed as an inset, where k_B is the Boltzmann constant, T the temperature, c the conversion constant from PSD voltage to bead displacement, α the force constant of the trap, and f the frequency. Here $\beta = 6\pi r\eta$ is the drag coefficient of the bead, which can be calculated based on a known bead diameter (r) and buffer viscosity (η). The power spectrum density distribution at a low frequency range (< 10 Hz) is sensitive to the air flow through the optical path, as well as other low frequency noises, which can be decreased by turning off the ventilation fan for the tweezer room and enclosing the optical path and components (Fig. 1.1B).

2.2. Flow cell assembly

The dual-trap optical tweezers have a horizontal optical layout (Fig. 1.1A and B) that contributes to the excellent mechanical stability and high spatio-temporal resolution of the instrument. However, this design necessitates a thin and vertical flow cell mounted on a motorized stage (Fig. 1.2A). We use a flow cell with one central and two auxiliary channels (Fig. 1.2B and C). The channels are laser engraved in two layers of nescofilm, sandwiched between two glass coverslips and sealed by heating (Fig. 1.2D). The central channel is used for optical trapping, while the auxiliary channels supply the two different kinds of beads required for the single-molecule experiments, typically streptavidin (SA)- and anti-digoxigenin (αDIG)-coated polystyrene beads. The beads are delivered from the auxiliary channels to the central channel through glass tubing. A different glass tube is also used to directly inject the remodeler solution into a small reaction area in the central channel. This method of protein injection conserves the precious remodeler sample and allows fast protein addition and removal, compared to an alternative approach in which the protein solution is flowed through the entire central channel. It also offers the advantage to add remodeler solution after a single DNA molecule is attached to two trapped beads.

Flow in the central channel and the protein injection tube is controlled by the pressure in the corresponding solution vials through a combination of solenoid valves. These valves regulate the influx or efflux of pressurized nitrogen in each vial. Flow of bead solutions in the auxiliary channels is achieved with the help of home-built, computer-controlled syringe pumps. However, during the single-molecule experiment, the flow in the central channel should be minimal (but not zero) to avoid perturbation of the experiment due to differential flow dragging forces applied to both trapped beads. The background flow in the central channel can be judged by the drifting velocity of a bead after released from the trap by turning off the trap. In general, a downstream background flow should be set before the tweezer experiment such that free beads only slowly drift in the direction from the tip of the protein injection tube to the tips of dispenser tubes. This default background flow (typically <1 μm/s) prevents the beads exiting from the dispenser tubes from drifting to the test area between tips of the two kinds of tubes and interfering with the single-molecule experiment.

Liquid in the flow cell and its connecting tubes should be free of air bubbles and contaminant particles. Air bubbles trapped in the flow cell can disturb the flow and introduce noise in the measured extension and

force signals. Therefore, air bubbles should be removed from the flow cell and connecting tubing before any tweezers experiments. Solution injected into the central channel should be clear and free of particles and other contaminants because they can be caught by the optical traps and disturb the measurements. Thus, buffers should be filtered and degassed. Protein samples often contain large contaminants or gel debris left from purification processes, which can be removed by spinning the protein solution after dilution into final reaction buffers. Filtering protein solution may cause protein depletion due to its absorption to the filter and is not recommended for cleaning remodeler solutions. Finally, at the end of tweezer experiment, the flow cell and all tubing should be thoroughly washed and filled with a solution of 0.01% sodium azide to prevent bacterial growth.

2.3. Tweezer calibration

The optical tweezers need to be calibrated to determine coefficients for the linear conversions from the mirror rotation angle to the trap separation and from the measured PSD voltages to bead displacements and forces (Moffitt et al., 2006). To calibrate trap separation, two polystyrene beads are held by the optical traps and separated in a step-wise manner. During this process, images of the two beads are taken by the CCD camera at each mirror position (Fig. 1.1A and C). Then the trap separation at each mirror position is measured as the distance between the centroids of the two bead images. Finally, the resultant plot of trap separation versus mirror rotation angle is linearly fit to get the slope and offset required to convert the mirror rotation angle to the trap separation. Such calibration is performed regularly (typically weekly) to correct any spontaneous drift of optical components.

In contrast, trap stiffness and the voltage-to-displacement conversion constants are generally determined for each trapped bead at the beginning of each experiment because these parameters slightly change among the beads with variable diameters. One first records the PSD response to the Brownian motion of the bead in each trap with a high bandwidth (typically 80 kHz) and then calculates the power spectrum density distribution of the acquired voltage signal after its baseline is subtracted (Fig. 1.3). For a particle confined in a harmonic potential, its displacement, in principle, should have a power spectrum density of Lorentzian distribution that is a function of the trap stiffness and the voltage-to-displacement conversion constant. A nonlinear fitting of the measured power spectrum density with the

Lorentzian function yields the two constants required for the calibration. In our experiments, typical trap stiffness and the conversion constant are ~0.2 pN/nm and 0.6 nm/mV, respectively, for a ~2 μm diameter polystyrene bead and ~300 mW laser power per trap. Note that it is beneficial to keep the stiffness of and bead diameters in both traps approximately equal to maximize the spatial resolution of the dual-trap optical tweezers.

3. REMODELER TRANSLOCATION ON BARE DNA

3.1. Experimental setup

To investigate motor translocation on bare DNA using optical tweezers, we have developed a tethered motor assay in collaboration with Cairns' group (Fig. 1.4A) (Sirinakis et al., 2011). Crucial to this assay is a DNA translocase fused with a tetracycline repressor TetR that can specifically bind to the tetO site in the middle of a DNA molecule stretched by the optical tweezers. Wild-type TetR is a homodimer and binds tetO with an association constant of $\sim 10^{11}\ M^{-1}$ (Orth, Schnappinger, Hillen, Saenger, & Hinrichs, 2000), which provides a strong anchor for motor translocation and force generation. This strong association can be reversed by adding tetracycline, which can serve as a control experiment to test the role of motor anchoring in the observed translocation signal. Once anchored on the DNA, motor translocation is accompanied by the formation of a DNA loop between the remodeler motor domain and TetR, which shortens the DNA end-to-end distance and increases the DNA tension detected by optical tweezers (Fig. 1.4B). Thus, motor translocation can be detected in real time (Fig. 1.4C).

3.2. Preparation of the DNA substrate

The 5063 bp DNA molecule contains a tetO site (tctatcattg atagg) incorporated into a pUC19 plasmid containing nine nucleosome position sequences (NPSs) "601" (pUC-N9). Construction of pUC-N9 will be described in Section 4.3. A polynucleotide containing a tetO site and its complementary strand are chemically synthesized, hybridized, and inserted into the modified plasmid between *Eco*RI and *Ban*II restriction sites. The resultant plasmid containing tetO site (tet-N9) is transformed into DH5α cells, amplified, and purified. The plasmid DNA is then digested with a *Sty*I restriction enzyme and labeled as detailed in the later section.

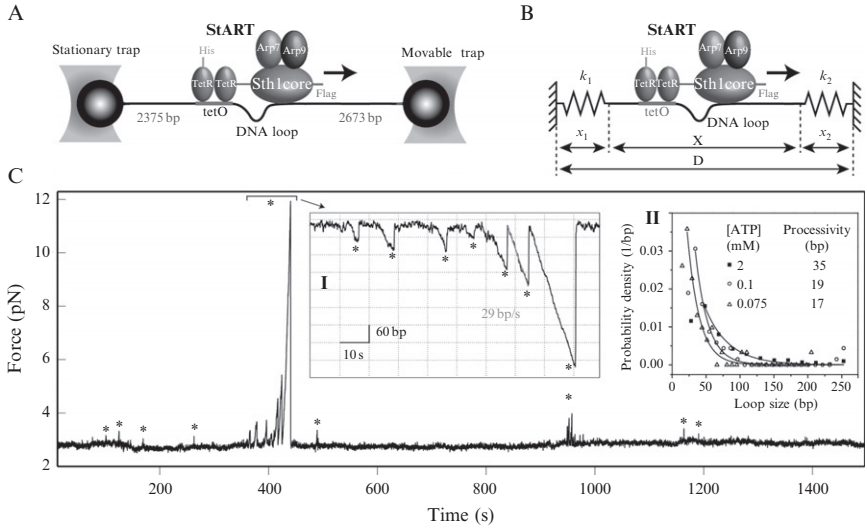

Figure 1.4 Tethered motor assay for remodeler translocation on bare DNA based on dual-trap high-resolution optical tweezers (Sirinakis et al., 2011). (A) Illustration of the experimental setup and the composition of the tethered minimal RSC complex (StART). Not drawn to scale. (B) Simplified diagram showing the principle of force and extension detection by optical tweezers. The two optical traps are equivalent to two microscopic springs with force constants k_1 and k_2. As the tethered motor (Sth1 core here) translocases DNA, it shortens the DNA end-to-end extension (X) and pulls the two beads away from their corresponding trap centers (increases in x_1 and x_2) while the trap separation (D) is kept fixed. (C) Time-dependent tension or length (inset I) of a single DNA molecule showing remodeler translocation and loop formation. The StART activities (marked by stars) contain continuous increases in force corresponding to remodeler translocation, followed by sudden drops to the baseline indicating disengagement of the remodeler translocation domain from the DNA. Signals tend to appear in a row, suggesting that the translocation domain can undergo multiple rounds of translocation and disengagement before the complex completely dissociates from the DNA molecule. Inset I shows the plot of DNA length (Section 5) versus time corresponding to the indicated force–time region. Translocation velocity and distance can be calculated based on this plot. Inset II shows probability density distributions of the translocation distance of StART at different ATP concentrations. The ATP-dependent processivity of the motor is listed in the inset.

3.3. Preparation of the tethered remodeler system

We first demonstrated the tethered motor assay using the minimal RSC complex (Sirinakis et al., 2011). The protein complex contains four subunits: Sth1 core, Arp7, Arp9, and TetR, designated as StART (Figs. 1.4A and 1.5A). Here, the two monomers in TetR are expressed from genes in the same plasmid under control of the same promoter, one fused with $Sth1_{(301\text{-}1097)}$-FLAG and the other labeled with an N-terminal His tag.

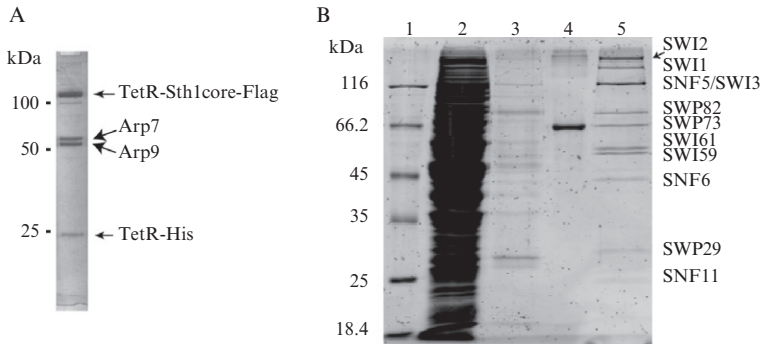

Figure 1.5 SDS gels of remodelers in different purification steps. Protein subunits in each purified complex are labeled on the right. (A) SDS gel of the purified tethered minimal RSC complex. (B) SDS gel of protein samples in different steps of SWI/SNF purification. The samples in different lanes are the protein marker with their molecular weights indicated on the left (lane 1), flow through of the IgG-Sepharose (lane 2), supernatant after the SWI/SNF-bound IgG-Sepharose is treated with TEV protease (lane 3), 100 ng BSA (lane 4), and final purified SWI/SNF complex (lane 5), respectively. The proteins are stained with SYPRO red (Invitrogen).

The two actin-related proteins (Arp7 and Arp9) are expressed from a second plasmid. Both plasmids are cotransformed into *Escherichia coli* BL21(DE3) RIL. The StART complexes are assembled in the cell and purified successively using Ni-NTA agarose resin (Qiagen) and anti-Flag M2 affinity gel (Sigma). The complexes are eluted with 3 × FLAG peptide (Sigma) and further refined by gel filtration on S200GL 10/300 (Amersham, GE) column. The pure complex is confirmed by SDS gel electrophoresis (Fig. 1.5A).

3.4. Procedure of single-molecule experiments on optical tweezers

3.4.1 Buffers

PBS buffer for bead dilution: 137 m*M* NaCl, 2.7 m*M* KCl, 8.1 m*M* Na_2HPO_4, 1.8 m*M* KH_2PO_4, pH 7.4.

The DNA translocation buffer for StART: 20 m*M* Tris–acetate, 10 m*M* magnesium acetate, 50 m*M* potassium acetate, 1 m*M* DTT, 6% glycerol, 0.1 mg/mL BSA, supplemented with typically 2 m*M* ATP.

3.4.2 Remodeler solution preparation

An aliquot of remodeler stock solution is diluted in the DNA translocation buffer just before the tweezer experiment and then spun at 4 °C at the highest speed of a bench-top centrifuge for 20 min. The supernatant is collected for the tweezer experiment.

3.4.3 Bead preparation

We typically use 1.87-μm-diameter streptavidin-coated and 2.17-μm-diameter anti-digoxigenin-coated polystyrene beads (Spherotech SVP-15-5 and DIGP-20-2, respectively). For applications requiring higher spatiotemporal resolution, beads with ~1 μm diameter or smaller should be used. However, these small beads tend to be more difficult to be visualized and trapped and lead to shorter tether lifetime than the big beads. The limited tether lifetime results from the photo damage induced by the high-intensity (>10 MW/cm^2) trapping light that produces free radicals to cleave the DNA-bead linkages (Landry, McCall, Qi, & Chemla, 2009). The photo damaging can be alleviated by adding an oxygen-scavenging system in the reaction buffer. But the oxygen-scavenging system tends to lower the pH of the protein solution, thus affecting the enzymatic activity. Fortunately, using the ~2-μm-diameter beads, we find that the DNA tether is generally stable enough to hold a low tension (<5 pN) for more than 20 min, without the presence of the oxygen-scavenging system. Therefore, these beads are mainly used in our remodeler translocation assays.

To prepare the beads for optical trapping, aliquots of the bead stock solutions are dispersed by either vortexing for 1 min or sonicating for 20 min. The DNA molecules can be bound to either SA beads or αDIG beads, with the latter as our choice here. The amount of DNA added to the bead solution should be optimized to allow pulling single DNA molecules, as detailed below.

3.4.4 Pull a single DNA

1. Wash and fill the central channel of the flow cell with the translocation buffer. To minimize protein absorption, the inner surface of the central channel and the protein injection tubing may be passivated by washing the channel and tubing with 0.5 mg/mL bovine serum albumin (5 × BSA) or 0.05% powdered milk and then thoroughly rinsing with the translocation buffer.
2. Dilute 2 μL of dispersed SA beads in 1 mL PBS buffer.
3. Bind the DNA molecules (tet-N9) to αDIG beads. About 5 ng of the DNA molecule is mixed with 20 μL dispersed αDIG beads and incubated for 20 min at room temperature to allow DNA binding. Then the DNA-bead solution is diluted in 1 mL of PBS buffer.
4. Inject the diluted DNA-αDIG bead solution and the SA bead solution to the auxiliary channels of the flow cell using 1 mL syringes.
5. Set the trap separation to the maximum.

6. Turn the stationary trap on and the movable trap off.
7. Move the flow cell through the motorized stage to position the tip of the dispenser tube for the DNA-bound beads in the vicinity of the stationary trap and capture a single DNA-αDIG bead.
8. Turn on the movable trap and similarly grab a single streptavidin-coated bead in this trap near the other dispenser tube.
9. Move the flow cell to position the trapped beads approximately in the middle of the central channel and between the dispenser tubes and the protein injection tube, an area designated as the test area.
10. Record Brownian motions for both trapped beads for about 20 s and calibrate the traps as described in Section 2.3.
11. Fish the DNA attached to the αDIG bead by moving the SA bead first close to and then away from the αDIG bead. In this process, the interacting force between the two beads is recorded. If one or multiple DNA molecules are captured by the SA bead, the force should increase as two beads are moving apart. Otherwise, the force remains zero during the separation. In this case, the fishing process will be repeated by moving the two beads successively closer, until formation of a DNA tether between the two beads is confirmed. Note that the fishing process can be facilitated by adding flow to stretch the DNA molecule on the αDIG bead toward the SA bead. However, if no DNA tether is found within a reasonable time period or about eight rounds of fishing, the αDIG bead may have no DNA molecule attached in the region accessible to the SA bead. Then both beads are released and Steps 5–11 will be repeated until a DNA tether is formed. We have automated this fishing process to facilitate the tweezer experiment (Fig. 1.1C).
12. Pull the DNA tether by separating the two traps at a uniform speed, typically 10–500 nm/s, until the tether breaks. If the DNA tether breaks in one step with a force drop to around zero or show a B-to-S transition around 65 pN (Smith, Cui, & Bustamante, 1996), the DNA tether is a single DNA molecule. Otherwise, the DNA tether may have multiple DNA molecules.
13. Test a total of around 10 different pairs of beads for DNA tether formation and perform the pulling experiment by repeating Steps 5–12.
14. Optimize the DNA amount bound to the αDIG beads if necessary by repeating Steps 3–13. Under the conditions for single-molecule experiments, the number of DNA molecules bound on a single bead (or more specifically the surface region accessible by the SA bead) follows a Poisson distribution, which has a maximum probability of 0.37 to have

a single DNA molecule for all bead pairs tested. Under this optimal condition, the probabilities to have zero and more than one DNA molecules are 0.37 and 0.26, respectively. If the probability to tether a single DNA molecule between a pair of beads is significantly lower than 0.37, one should increase or decrease the amount of DNA bound to the αDIG beads to make the single-molecule experiments more efficient.

3.4.5 Single remodeler translocation on bare DNA

15. Add the clean remodeler solution prepared in Section 3.4.2 into the 0.5-mL microcentrifuge tube connected to the protein injection tube (Fig. 1.2A).
16. Stretch a DNA tether to a tension of interest, typically around 3 pN. Then inject the protein solution into the test area in the central channel. The protein solution flow can exert a drag force on two beads (typically a few pN) and can be used to judge the flow rate (~50 μm/s/pN). Stop the flow after about 30 s when the test area is filled with the remodeler solution.
17. Measure the activity of the enzyme in real time while keeping the trap separation fixed for typically 20 min. The translocation signals are seen as spikes in which the force linearly increases followed by a sudden drop to the baseline (Fig. 1.4C). Record data at 5 kHz to a hard disk.
18. Confirm a single DNA molecule by pulling the tether to high forces as described in Step 12.
19. Collect more translocation signals by repeating Steps 16–18 using different pairs of beads.

4. NUCLEOSOME-DEPENDENT REMODELER TRANSLOCATION

4.1. Experimental design

In contrast with the tethered minimal RSC complex, full complexes of SWI/SNF and RSC can target histones and pump DNA around the histone octamer (Zhang et al., 2006). Both remodelers are comprised of more than 10 different subunits and contain histone binding domains that serve as DNA anchors to constrain the DNA loop while their translocases pump DNA toward the histone octamer (Fig. 1.6A). Thus, DNA translocation properties of the full remodeler complexes can be similarly measured on nucleosomal DNA templates and compared with those obtained on bare DNA templates. These comparisons can reveal the effects of the nucleosome substrate and

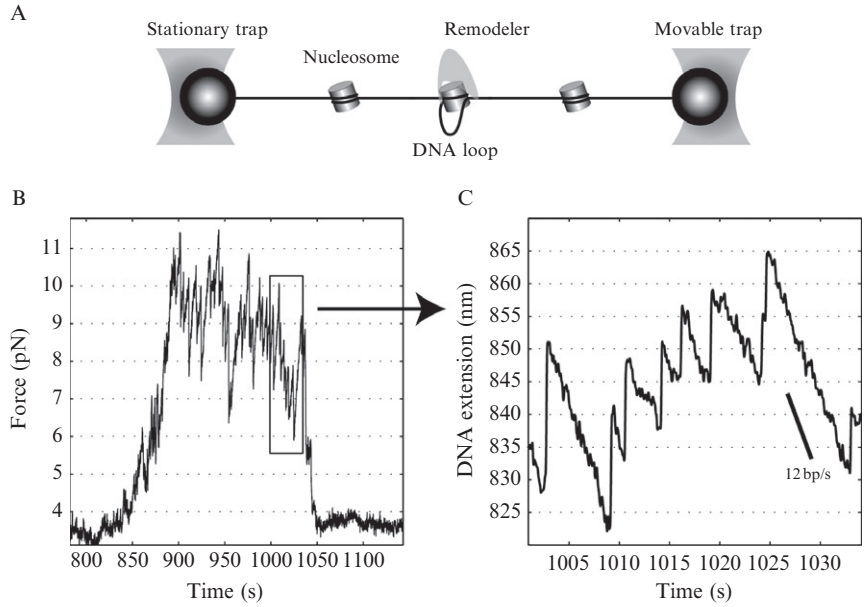

Figure 1.6 Nucleosome-dependent RSC translocation (Sirinakis et al., 2011). (A) Diagram of the experimental setup. (B) Time-dependent tension of the nucleosomal DNA template showing RSC translocation. The repetitive RSC-induced DNA loop formation and dissipation is caused by DNA translocation of a single RSC complex after bound on the nucleosome. (C) Time-dependent DNA length corresponding to the boxed area in (B).

other protein subunits of remodelers on DNA translocation (Fig. 1.6B and C). In the following, we will describe the single-molecule experiment on the nucleosomal DNA template.

It may be advantageous to put a single nucleosome on a long DNA molecule to test the nucleosome-dependent remodeler translocation. This single-nucleosome DNA template can avoid remodeler collisions into neighboring nucleosomes during translocation. Moreover, the experimental noise is generally lower on the single-nucleosome template than on the nucleosomal array template because fast nucleosomal DNA unwrapping–rewrapping fluctuations on histone surfaces add to the measured noises in a nucleosome number-dependent manner. However, the single-nucleosome template is difficult to make (Zhang et al., 2006), partly because a single nucleosome on a long DNA molecule is not so stable under the single-molecule conditions. Furthermore, the chance to observe translocation signals is relatively low on a single nucleosome, probably because the nucleosome-dependent loop formation is only one of many pathways

in a remodeler-catalyzed remodeling reaction. To overcome these difficulties, we use a special nucleosomal array in our single-molecule experiment. This array consists of nine tandem repeats of 258 bp DNA containing the "601" nucleosome-positioning sequence (Lowary & Widom, 1998). The large spacing between nucleosomes deposited on this DNA molecule allows enough bare DNA on both sides of a nucleosome for remodeler translocation.

4.2. Purification of SWI/SNF and RSC

SWI/SNF and RSC are purified endogenously using the tandem affinity purification (TAP) method as previously reported (Smith, Horowitz-Scherer, Flanagan, Woodcock, & Peterson, 2003; Wittmeyer, Saha, & Cairns, 2004). In this method, one of the protein subunits is added with a TAP-tag at its carboxyl-terminal. The TAP-tag contains a calmodulin-binding peptide, a TEV protease cleavage site, and protein A. The TAP-tag is fused to the SWI2 subunit of SWI/SNF and the Rsc2 subunit of RSC, respectively. Starting from yeast cell extracts, both complexes are first bound to IgG-Sepharose, cut from the resin by TEV protease, then bound to calmodulin beads with calcium, and finally eluted from the beads in the presence of EGTA, yielding pure remodeler complexes (Fig. 1.5B).

4.3. Preparation of the DNA containing NPSs (Zhang et al., 2006)

1. Make the DNA molecule with the following multicloning sequence:

```
     EcoRI                BanII    AvaI                PstI     StyI      HindIII
CAGTGAATTCACCGTCTAAGATCTGATTCGAGCCCGGTACTCGGGGATCCTCTAGAGTAGACCTGCAGGCTCAGCCTTGGATGATGCAAGCTTGGCG
GTCACTTAAGTGGCAGATTCTAGACTAAGCTCGGGCCATGAGCCCCTAGGAGATCTCATCTGGACGTCCGAGTCGGAACCTACTACGTTCGAACCGC
```

2. Clone the sequence into the pUC19 plasmid between the *Eco*RI and *Hin*dIII sites, generating a pUC19 plasmid variant with a modified multicloning site.
3. Synthesize the DNA molecules containing the 258 bp sequence repeat with nonpalindromic *Ava*I restriction sites (CTCGGG) on both ends. Clone the DNA fragment into the pUC19 variant through the *Ava*I site, generating a sufficient amount (> 50 μg) of the new plasmid pUC-N1 containing one NPS repeat.
4. Digest the pUC-N1 plasmid with *Ava*I and purify the NPS repeat sequence using agarose gel electrophoresis.

5. Ligate the NPS repeat sequence and separate the resultant DNA ladder by agarose gel electrophoresis (Fig. 1.7A). Purify the tandem repeats containing the required number of NPSs from the gel.
6. Clone the purified tandem NPS repeats back into the pUC19 plasmid variant through the *Ava*I site, generating the required plasmid DNA sequences containing defined number of NPS repeats. Purify the plasmid DNA using the standard plasmid purification method (such as the Qiagen plasmid purification kits) and further concentrate the DNA by ethanol precipitation.

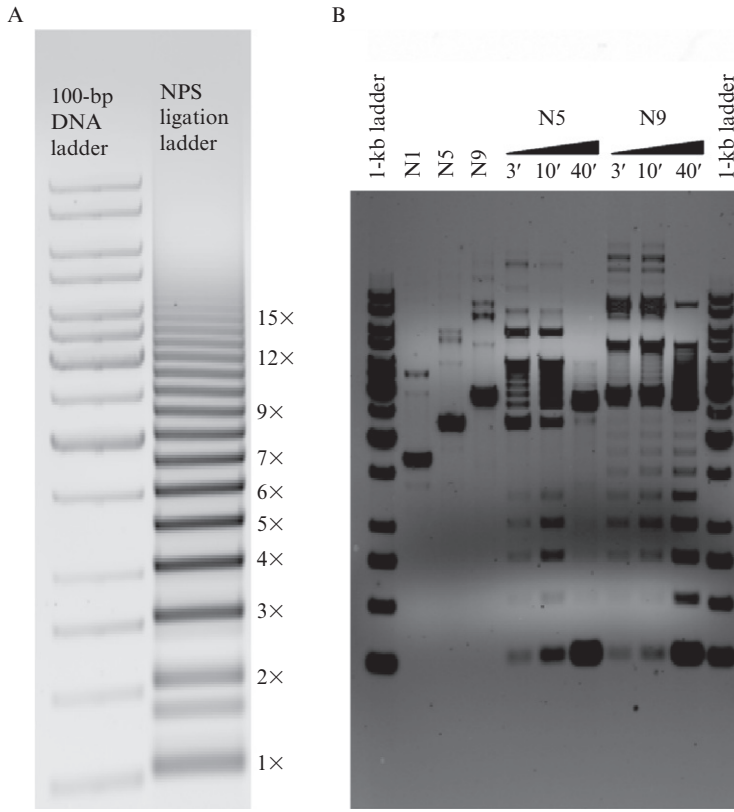

Figure 1.7 Construction of the tandem repeats of nucleosome-positioning sequences (NPSs). (A) Agarose gel of the NPS ladder formed by ligation of NPS monomers (258 bp). The number of NPS repeats is indicated on the right. (B) Agarose gel of the plasmids containing 1 (N1), 5 (N5), and 9 (N9) NPS repeats purified from *E. coli* and their limited digested products by *Ava*I restriction enzyme. *Ava*I digestion for a time period of 3, 10, and 40 min gradually releases multiple NPS repeats or monomers. The maximum number of bands in the NPS ladder indicates the number of NPS repeats in the plasmid.

7. Confirm the number of NPS repeats in the plasmids by limited *Ava*I digestion (Fig. 1.7B).

4.4. DNA labeling with biotin and digoxigenin by DNA polymerase extension

1. Digest 40 μg of pUC-N9 DNA plasmid with 20 units of *Sty*I restriction enzyme (New England Biolabs, MA) in 50 μL of 1 × NEB Buffer 3 (50 m*M* Tris–HCl, 100 m*M* NaCl, 10 m*M* $MgCl_2$, and 1 m*M* DTT, pH 7.9) containing 0.1 mg/mL BSA. Incubate overnight at 37 °C.
2. Add to the above reaction mixture 4 μL of 1 m*M* digoxigenin-dUTP (Roche), 8 μL of 0.4 m*M* biotin-dATP (Roche), 0.7 μL of 10 m*M* dCTP, 0.7 μL of 10 m*M* dGTP, 3 μL of 10 × EcoPol Buffer (NEB), 2.6 μL ddH_2O, and 1 μL Klenow (Exo^-) (NEB). Incubate the 70 μL mixture at 37 °C for 1 h. The reaction adds two biotin moieties at one end of the DNA and two digoxigenin moieties at the other end.
3. Purify the labeled DNA by phenol:chloroform extraction and ethanol precipitation. Store the DNA in 20 μL TE buffer (10 m*M* Tris–HCl, 1 m*M* EDTA, pH 8.0).

4.5. Nucleosome reconstitution by salt-dialysis method

1. Mix 10 μg of the labeled pUC-N9 DNA with 2.5, 2.8, and 3.2 μg of histone octamer in three 2 *M* NaCl solutions with a final 100 μL volume. The histone octamer is purified from chicken erythrocytes.
2. Transfer the mixtures to "Slide-a-Lyzer" mini dialysis buckets (Pierce) and dialyze at 4 °C against 1500 mL Tris–EDTA buffer (10 m*M* Tris–HCl, pH 8.0, 0.25 m*M* EDTA) containing 1.5 *M* NaCl for 3 h.
3. Dialyze the reconstitution mixtures against the Tris–EDTA buffer containing successively lower concentrations of NaCl, that is, 1.0 *M*, 0.8 *M*, 0.6 *M*, and finally 2.5 m*M*, each for 3 h at 4 °C.
4. Collect the sample and store at 4 °C.

The quality of the reconstituted nucleosomal arrays is crucial for chromatin structure and remodeling studies. In the following, we will use atomic force microscopy (AFM) imaging and single-molecule manipulation method to assess the nucleosome number distribution on the DNA molecules. Whereas undersaturated nucleosome arrays can be used in some experiments, oversaturated arrays should be avoided because noncanonical nucleosomal structures may be formed on these templates. We normally make at least three reconstituted nucleosomal arrays at a time with slightly

different histone-to-DNA ratios, which allow selection of the arrays with proper nucleosome occupancy for single-molecule experiments.

4.6. AFM imaging of nucleosomal arrays

The nucleosomal array is fixed by glutaraldehyde before AFM imaging. To fix the array, the reconstituted sample is further dialyzed. First, the array is dialyzed against 1 m*M* EDTA, pH 8.0; then against 1 m*M* EDTA, 0.1% fresh glutaraldehyde, pH 7.7; finally against 1 m*M* EDTA, pH 7.6. Each step of dialysis should be at 4 °C for 6 h. The nucleosomal array is imaged by a MultiMode NanoScope V AFM (Veeco Instruments) with a type E scanner. First, the fresh mica surface is treated with spermidine by adding 10 μL of 100 m*M* spermidine, rinsed with ddH_2O, and dried with nitrogen flow. Then about 5 ng of fixed nucleosomal DNA in 20 μL EDTA buffer, pH 7.6 is added to the treated mica surface and imaged using the AFM in a tapping mode. The silicon cantilever (Nanosensors) used for imaging has a resonance frequency of 260–410 kHz and a force constant of 21–78 N/m. Representative images are shown in Fig. 1.8, from which the average number and positioning of nucleosomes on the DNA sequence can be scored.

4.7. Pulling nucleosomal arrays

The nucleosomal DNA is attached to the two beads and pulled similar to the bare DNA described in Section 3.4.4. A representative force–extension curve (FEC) is shown in Fig. 1.9A, in which each rip corresponds to the mechanical disruption of a nucleosome core particle on the DNA molecule. Thus, the number of nucleosomes on each nucleosomal array can be counted as the number of rips in the measured FECs. Furthermore, canonical nucleosomes show extension changes centered at 70 bp (Fig. 1.9B) and disruption forces around 23 pN (Fig. 1.9C), consistent with the previous report (Brower-Toland et al., 2002). Significant deviation from these distributions may indicate improper nucleosome reconstitution.

4.8. Nucleosome-dependent SWI/SNF and RSC translocation

The translocation is performed in different buffers for both remodelers: 20 m*M* Tris–HCl (pH 8.0), 125 m*M* NaCl, 5 m*M* $MgCl_2$, 1% glycerol, 0.2 m*M* DTT, 0.1 mg/mL BSA, and 0.05% NP-40 for SWI/SNF, and 20 m*M* HEPES (pH 7.6), 100 m*M* potassium acetate, 5 m*M* magnesium acetate, 1% glycerol, 0.2 m*M* DTT, 0.1 mg/mL BSA, and 0.05% NP-40 for RSC. The typical nominal remodeler concentration (the remodeler

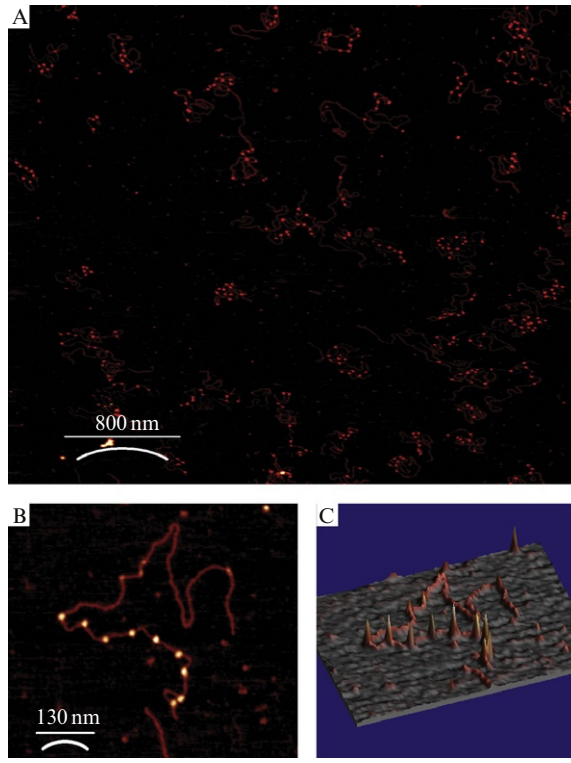

Figure 1.8 AFM images of the reconstituted nucleosomal arrays. (A) AFM image of the nucleosome arrays on the plasmid DNA containing nine tandem repeats of NPSs (pUC-N9). Nucleosomes (bright spots) are mainly formed on NPSs located at half of the DNA molecule, with the other half being plasmid DNA free of nucleosomes. (B) Close-up view of a single nucleosomal array containing nine uniformly spaced nucleosomes. (C) The 3D image corresponding to the image in (B). The average height of nucleosomes is 3.1 nm.

concentration before adding to the flow cell) is 2–20 n*M*. DNA translocation activities of SWI/SNF and RSC are tested on the nucleosomal DNA in a way similar to that of StART on bare DNA (Figs. 1.4A and 1.6A). Because histones can dissociate from DNA over time in a force-dependent manner, the experiment is normally carried out at a low tension (2–5 pN) to minimize spontaneous nucleosome disassembly and to facilitate loop formation. We found that SWI/SNF and RSC have similar nucleosome-dependent translocation properties (Zhang et al., 2006), with a trace shown for RSC in Fig. 1.6B.

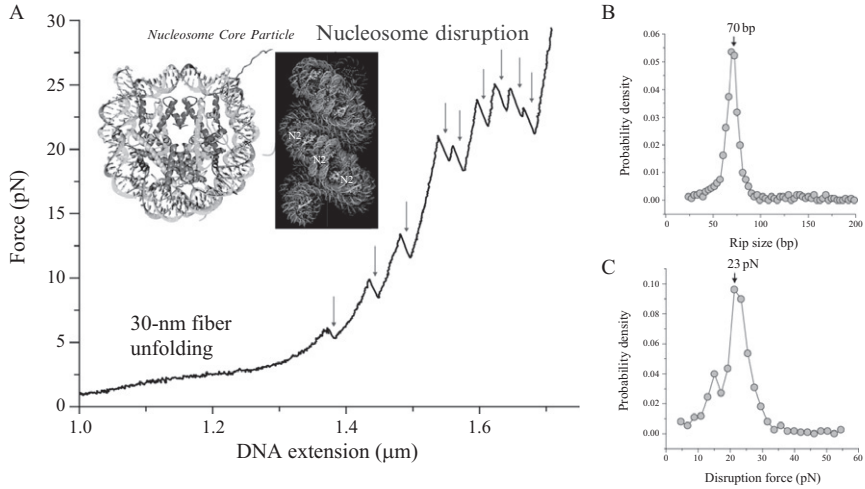

Figure 1.9 Mechanical disruption of single nucleosomal arrays. (A) Force–extension curve (FEC) of a single nucleosomal array with nine nucleosomes obtained by pulling the array at a rate of 100 nm/s. Individual events of nucleosome disruption are indicated by arrows. Here, each rip corresponds to discontinuous nucleosomal DNA unwrapping from the histone surface in a high-force regime (>5 pN). In the low-force regime (<5 pN), the FEC shows a force plateau around 2.5 pN. This plateau is reversible in the low-force regime and distinct only in the presence of approximately saturated nucleosomal array and >2 m*M* magnesium in the buffer. Compared to previous results (Kruithof et al., 2009), we conclude that this plateau is a signature of reversible folding and unfolding of the 30-nm fiber. The inset shows the crystal structure of the nucleosome core particle (Luger, Mader, Richmond, Sargent, & Richmond, 1997) and a model of the 30-nm fiber (Schalch, Duda, Sargent, & Richmond, 2005). (B) Histogram distribution of the DNA length released when nucleosomes are disrupted. The average length is 70 bp as indicated. (C) Histogram distribution of the force to disrupt nucleosomes measured from the rips in the FECs. The average force is 23 pN as indicated.

5. DATA ANALYSIS

Data corresponding to individual tethers are saved in a binary format in separate files, including calibration parameters, PSD signals, rotary mirror angles, and other experimental information such as pulling velocities. These data are read by a MATLAB program to calculate the tether extension and tension and displayed in plots of the FEC and the time-dependent extension, force, and trap separation. Only the data obtained on single DNA molecules are further analyzed. To determine the actual translocation distance of a remodeler along the DNA contour from the measured DNA extension and tension, we calculate the contour length of the portion of the DNA

directly stretched by optical traps, based on the worm-like-chain model of a DNA molecule. The time-dependent contour length trace is typically mean filtered to 20 Hz and presented (Figs. 1.4C and 1.6C). To unambiguously identify remodeler translocation signals, the instantaneous velocity of remodeler translocation is calculated by a linear regression of the contour length trace with a moving Gaussian function as weight. The standard deviation of the Gaussian function varies with the noise level of the baseline in the range of 0.5–2 s. Contour length changes are considered as signals only when their corresponding absolute instantaneous velocities exceed a threshold value (1–4 bp/s). This approach typically identifies looping signals >10 bp and smoothes out possible smaller signals. Once a signal is identified, the corresponding translocation velocities are calculated by linear regression of the pause-free regions, and the translocation distance is scored as the length difference between the starting and ending points of the translocation signal.

ACKNOWLEDGMENTS

We thank Drs. Brad Cairns, Cedric Clapier, and Craig Peterson for contributing to this research. The research in the Zhang lab has been funded by the Albert Einstein College of Medicine, the Alexandrine and Alexander L Sinsherimer Fund, the Kingsley Fund, and Yale University.

REFERENCES

Abbondanzieri, E. A., Greenleaf, W. J., Shaevitz, J. W., Landick, R., & Block, S. M. (2005). Direct observation of base-pair stepping by RNA polymerase. *Nature*, *438*, 460–465.

Amitani, I., Baskin, R. J., & Kowalczykowski, S. C. (2006). Visualization of Rad54, a chromatin remodeling protein, translocating on single DNA molecules. *Molecular Cell*, *23*, 143–148.

Boeger, H., Griesenbeck, J., Strattan, J. S., & Kornberg, R. D. (2004). Removal of promoter nucleosomes by disassembly rather than sliding in vivo. *Molecular Cell*, *14*, 667–673.

Bowman, G. D. (2010). Mechanisms of ATP-dependent nucleosome sliding. *Current Opinion in Structural Biology*, *20*, 73–81.

Brower-Toland, B. D., Smith, C. L., Yeh, R. C., Lis, J. T., Peterson, C. L., & Wang, M. D. (2002). Mechanical disruption of individual nucleosomes reveals a reversible multistage release of DNA. *Proceedings of the National Academy of Sciences of the United States of America*, *99*, 1960–1965.

Bustamante, C., Cheng, W., & Mejia, Y. X. (2011). Revisiting the central dogma one molecule at a time. *Cell*, *144*, 480–497.

Cairns, B. R. (2005). Chromatin remodeling complexes: Strength in diversity, precision through specialization. *Current Opinion in Genetics & Development*, *15*, 185–190.

Clapier, C. R., & Cairns, B. R. (2009). The biology of chromatin remodeling complexes. *Annual Review of Biochemistry*, *78*, 273–304.

Flaus, A., Martin, D. M., Barton, G. J., & Owen-Hughes, T. (2006). Identification of multiple distinct Snf2 subfamilies with conserved structural motifs. *Nucleic Acids Research*, *34*, 2887–2905.

Gittes, F., & Schmidt, C. F. (1998). Interference model for back-focal-plane displacement detection in optical tweezers. *Optics Letters*, *23*, 7–9.

Gkikopoulos, T., Schofield, P., Singh, V., Pinskaya, M., Mellor, J., Smolle, M., et al. (2011). A role for Snf2-related nucleosome-spacing enzymes in genome-wide nucleosome organization. *Science*, *333*, 1758–1760.

Greenleaf, W. J., Woodside, M. T., Abbondanzieri, E. A., & Block, S. M. (2005). Passive all-optical force clamp for high-resolution laser trapping. *Physical Review Letters*, *95*, 2081021–2081024.

Hamiche, A., Sandaltzopoulos, R., Gdula, D. A., & Wu, C. (1999). ATP-dependent histone octamer sliding mediated by the chromatin remodeling complex NURF. *Cell*, *97*, 833–842.

Hargreaves, D. C., & Crabtree, G. R. (2011). ATP-dependent chromatin remodeling: Genetics, genomics and mechanisms. *Cell Research*, *21*, 396–420.

Konev, A. Y., Tribus, M., Park, S. Y., Podhraski, V., Lim, C. Y., Emelyanov, A. V., et al. (2007). CHD1 motor protein is required for deposition of histone variant h3.3 into chromatin in vivo. *Science*, *317*, 1087–1090.

Kruithof, M., Chien, F. T., Routh, A., Logie, C., Rhodes, D., & van Noort, J. (2009). Single-molecule force spectroscopy reveals a highly compliant helical folding for the 30-nm chromatin fiber. *Nature Structural & Molecular Biology*, *16*, 534–540.

Landry, M. P., McCall, P. M., Qi, Z., & Chemla, Y. R. (2009). Characterization of photoactivated singlet oxygen damage in single-molecule optical trap experiments. *Biophysical Journal*, *97*, 2128–2136.

Langst, G., Bonte, E. J., Corona, D. F. V., & Becker, P. B. (1999). Nucleosome movement by CHRAC and ISWI without disruption or trans-displacement of the histone octamer. *Cell*, *97*, 843–852.

Lowary, P. T., & Widom, J. (1998). New DNA sequence rules for high affinity binding to histone octamer and sequence-directed nucleosome positioning. *Journal of Molecular Biology*, *276*, 19–42.

Luger, K., Mader, A. W., Richmond, R. K., Sargent, D. F., & Richmond, T. J. (1997). Crystal structure of the nucleosome core particle at 2.8 angstrom resolution. *Nature*, *389*, 251–260.

Mizuguchi, G., Shen, X. T., Landry, J., Wu, W. H., Sen, S., & Wu, C. (2004). ATP-driven exchange of histone H2AZ variant catalyzed by SWR1 chromatin remodeling complex. *Science*, *303*, 343–348.

Moffitt, J. R., Chemla, Y. R., Izhaky, D., & Bustamante, C. (2006). Differential detection of dual traps improves the spatial resolution of optical tweezers. *Proceedings of the National Academy of Sciences of the United States of America*, *103*, 9006–9011.

Moffitt, J. R., Chemla, Y. R., Smith, S. B., & Bustamante, C. (2008). Recent advances in optical tweezers. *Annual Review of Biochemistry*, 77, 205–228.

Nugent-Glandorf, L., & Perkins, T. T. (2004). Measuring 0.1-nm motion in 1 ms in an optical microscope with differential back-focal-plane detection. *Optics Letters*, *29*, 2611–2613.

Orth, P., Schnappinger, D., Hillen, W., Saenger, W., & Hinrichs, W. (2000). Structural basis of gene regulation by the tetracycline inducible Tet repressor-operator system. *Nature Structural Biology*, *7*, 215–219.

Papamichos-Chronakis, M., & Peterson, C. L. (2008). The Ino80 chromatin-remodeling enzyme regulates replisome function and stability. *Nature Structural & Molecular Biology*, *15*, 338–345.

Pyle, A. M. (2008). Translocation and unwinding mechanisms of RNA and DNA helicases. *Annual Review of Biophysics*, *37*, 317–336.

Saha, A., Wittmeyer, J., & Cairns, B. R. (2002). Chromatin remodeling by RSC involves ATP-dependent DNA translocation. *Genes & Development*, *16*, 2120–2134.

Schalch, T., Duda, S., Sargent, D. F., & Richmond, T. J. (2005). X-ray structure of a tetranucleosome and its implications for the chromatin fibre. *Nature*, *436*, 138–141.

Sinha, M., Watanabe, S., Johnson, A., Moazed, D., & Peterson, C. L. (2009). Recombinational repair within heterochromatin requires ATP-dependent chromatin remodeling. *Cell*, *138*, 1109–1121.

Sirinakis, G., Clapier, C. R., Gao, Y., Viswanathanc, R., Cairns, B. R., & Zhang, Y. L. (2011). The RSC chromatin remodeling ATPase translocates DNA with high force and small step size. *The EMBO Journal*, *30*, 2364–2372.

Smith, C. L., Cui, Y., & Bustamante, C. (1996). Overstretching B-DNA: The elastic response of individual double-stranded and single-stranded DNA molecules. *Science*, *271*, 795–799.

Smith, C. L., Horowitz-Scherer, R., Flanagan, J. F., Woodcock, C. L., & Peterson, C. L. (2003). Structural analysis of the yeast SWI/SNF chromatin remodeling complex. *Nature Structural Biology*, *10*, 141–145.

Smith, C. L., & Peterson, C. L. (2005). ATP-dependent chromatin remodeling. *Current Topics in Developmental Biology*, *65*, 115–148.

Whitehouse, I., Stockdale, C., Flaus, A., Szczelkun, M. D., & Owen-Hughes, T. (2003). Evidence for DNA translocation by the ISWI chromatin-remodeling enzyme. *Molecular and Cellular Biology*, *23*, 1935–1945.

Wittmeyer, J., Saha, A., & Cairns, B. (2004). DNA translocation and nucleosome remodeling assays by the RSC chromatin remodeling complex. *Methods in Enzymology*, *377*, 322–343.

Zhang, Y. L., Smith, C. L., Saha, A., Grill, S. W., Mihardja, S., Smith, S. B., et al. (2006). DNA translocation and loop formation mechanism of chromatin remodeling by SWI/SNF and RSC. *Molecular Cell*, *24*, 559–568.